Supersymmetry reach of the Fermilab Tevatron via trilepton, like-sign dilepton, and dilepton plus tau jet signatures

Konstantin T. Matchev

Theoretical Physics Department, Fermi National Accelerator Laboratory, Batavia, Illinois 60510

Damien M. Pierce

Physics Department, Brookhaven National Laboratory, Upton, New York 11973

We determine the Fermilab Tevatron's reach in supersymmetric parameter space in trilepton, like-sign dilepton, and dilepton plus tau-jet channels. We critically study the standard model background processes. We find larger backgrounds and, hence, significantly smaller reach regions than recent analyses. We identify the major cause of the background discrepancy. We improve signal-to-noise by introducing an invariant mass cut which takes advantage of a sharp edge in the signal dilepton invariant mass distribution. Also, we independently vary the cuts at each point in SUSY parameter space to determine the set which yields the maximal reach. We find that this cut optimization can significantly enhance the Tevatron reach.
[S0556-2821(99)05717-3]

PACS number(s): 11.30.Pb, 24.10.Lx

I. INTRODUCTION

For at least the next 6 years the Fermilab Tevatron will remain the highest energy collider in the world. The Tevatron upgrade will provide an exciting opportunity for discovering physics beyond the standard model. The hadronic environment at the Tevatron presents a number of challenges and extracting new physics signals can be difficult. In this respect, signatures with low standard model (especially QCD) backgrounds are extremely valuable, as they may provide our best opportunity for finding new physics before the CERN Large Hadron Collider (LHC) turns on.

Supersymmetry (SUSY) [1] has been fascinating particle physicists for more than 25 years. It seems an intrinsic component of theories unifying gravity and gauge interactions such as string theory, M theory or supergravity, has played an important role in the ''second string revolution'' of the last few years. The minimal supersymmetric extension of the standard model (MSSM) is a well defined, renormalizable and calculable model, which offers a technical solution to the hierarchy problem [2], if the masses of the superpartners of the standard model particles are of order the weak scale. Our belief that supersymmetry might be relevant at energy scales accessible at present colliders is reinforced by the successful gauge coupling unification [3]. Also, due to decoupling the MSSM is generally in agreement with precision data [4]. In addition, a generic prediction of the MSSM is the existence of a light Higgs boson [5,6], which is preferred by fits to data [7]. In summary, the MSSM is a well-motivated extension of the standard model, which has a very rich and interesting phenomenology [8].

Because of the relatively low [compared to the LHC or Next Linear Collider (NLC)] center of mass energy and integrated luminosity in run II, the Tevatron is able to explore only the low end of the superpartner spectrum. Searches for colored superpartners (squarks and gluinos) are done in jetty channels, which suffer from relatively large backgrounds. On the other hand, $SU(2)$-gaugino pair production leads to a unique clean trilepton signature [9,10], which has been considered a ''gold-plated'' mode for SUSY discovery at the Tevatron. Both the Collider Detector at Fermilab (CDF) and D0 Collaborations have already performed run I trilepton analyses [11]. In light of the importance of this channel in run II, it is clamant to:

(1) have a reliable estimate of both signal and background rates. We would prefer to determine background rates from data, but until run II we primarily rely on Monte Carlo simulations. ISAJET and PYTHIA have been two of the most commonly used event generators in SUSY analyses. While there is a reasonable agreement for the signal, PYTHIA-based studies [10,12] have obtained larger values for the trilepton backgrounds (mainly WZ and ZZ) than ISAJET-based analyses [9,13,14]. This discrepancy was noticed and discussed in the TeV 2000 Report [15], but was attributed to the different lepton rapidity cuts used in the various analyses.

(2) use an optimized set of cuts, which will maximize the Tevatron reach. A first step in this direction was taken in Refs. [14], where softer lepton p_T cuts have been proposed, thus enhancing signal over background throughout a large part of parameter space.

(3) include next-to-leading order (NLO) corrections to the production cross sections. The corrections to diboson production [16], $t\bar{t}$ production [17] and Drell-Yan [18], have been known for some time, and the corrections will soon be available for chargino-neutralino production as well [19].

(4) identify regions of parameter space where the reach via the trilepton signature is diminished and try to find an alternative search strategy in those regions. An example of this sort is the large $\tan\beta$ region with light sleptons, where one often finds that both the chargino and the neutralino decay predominantly to tau leptons. Then the trilepton signal has a very small branching ratio *and* the leptons are quite soft, which can make it unobservable at run II, even for chargino masses as low as 100 GeV. In this case it is possible to recover sensitivity by considering alternative signa-

tures with tau jets [12]. Another alternative to the trilepton signature is the inclusive like-sign dilepton channel [20], where the signal acceptance is increased by not requiring the odd-sign lepton in the event.

In this paper, we shall try to address most of these issues. We perform detailed Monte Carlo simulations of signal and background using both PYTHIA and ISAJET and explain the cause for the largest background discrepancy. We also determine the maximum reach by applying an optimal set of cuts at each point in the supersymmetric parameter space.

Also, we make use of the presence of a sharp edge in the dilepton invariant mass distribution of the signal by applying a more restrictive invariant mass cut, thus reducing the WZ and ZZ backgrounds. As the NLO corrections to gaugino production are not yet available, we conservatively use leading order cross sections for all processes. Preliminary results [19] show that the k-factor is roughly the same for both signal and background. Hence, we expect that the Tevatron reach will be improved once NLO corrections are incorporated.

We show our results for the discovery potential of the upgraded Tevatron in the so-called minimal supergravity model (MSUGRA) [29]. This model has universal soft parameter boundary conditions at the grand unification scale, and its spectrum displays characteristic properties. For example, the imposition of electroweak symmetry breaking results in[1] $|\mu| > M_2$, so that the lightest chargino and lightest two neutralinos are gaugino-like. Also, the squark and slepton masses are generation independent, except at large $\tan\beta$ where the third generation masses can be lighter. This model has five input parameters: the scalar mass M_0, the gaugino mass $M_{1/2}$, the A-term A_0, the ratio of vacuum expectation values $\tan\beta$, and the sign of the μ term. We show results for $\mu > 0$ and $A_0 = 0$.

We adopt a signature driven approach by comparing and contrasting three of the cleanest channels for run II—the trilepton (3L) [9,10], like-sign dilepton (2L) [20] and dilepton plus tau jet (2L1T) [12] channels. The 3L channel is the long studied ''gold-plated'' channel. The 2L channel has larger signal acceptance compared to 3L, but it is not *a priori* clear whether this advantage will be spoiled by the concomitant increase in the background. The 2L1T channel is known to be important at large $\tan\beta$, where the right-handed tau-slepton is lighter than the first two generation sleptons. Here we will discuss this channel at small $\tan\beta$ as well.

We describe in detail our numerical analysis in Sec. II, where we also describe the cuts we consider for each signature. We discuss all non-negligible backgrounds and their evaluation in Sec. III. Then, in Sec. IV, we map our results for the Tevatron reach onto the parameter space of the MSUGRA model. We reserve Sec. V for our conclusions.

II. ANALYSIS

In this section we describe our numerical analysis. We use PYTHIA v. 6.115 [21] and ISAJET v. 7.42 [22] for event gen-

eration, and the SHW v. 2.2 detector simulation package [23], which mimics an average of the CDF and D0 Run II detector performance. We use PYTHIA for the background determinations, together with TAUOLA [24] to account for the correct (on average) tau polarization in tau decays. We have made several modifications in SHW, which are appropriate for our purposes:

(1) We extend the tracking coverage to $|\eta| < 2.0$, which increases the electron and muon acceptance, as is expected in run II [25]. For muons with $1.5 < |\eta| < 2.0$, we apply the same fiducial efficiency as for $1.0 < |\eta| < 1.5$. However, we still require that tau jets are reconstructed only up to $|\eta| < 1.5$.

(2) We retain the existing electron isolation requirement and add a muon isolation requirement $I < 2$ GeV, where I is the total transverse energy contained in a cone of size $\Delta R = \sqrt{\Delta \phi^2 + \Delta \eta^2} = 0.4$ around the muon.

(3) We increase the jet cluster E_T cut to 15 GeV and correct the jet energy for muons. We also add a simple electron/photon rejection cut $E_{em}/E_{had} < 10$ to the jet reconstruction algorithm, where E_{em} (E_{had}) is the cluster energy from the electromagnetic (hadronic) calorimeter.

(4) We correct the calorimeter $\not{E}_T$ for muons.

(5) We account for an incorrect assignment of neutralino particle id's in the ISAJET translation of STDHEP v. 4.05 [26].[2]

The addition of the muon isolation cut and the jet E_{em}/E_{had} cut allows us to uniquely resolve the ambiguity arising in SHW v. 2.2, when a lepton and a jet are very close.

As we mentioned in the Introduction, we show results for three of the cleanest SUSY channels in run II at the Tevatron—trileptons, inclusive like-sign dileptons and dileptons plus a tau jet. In our analysis we consider both channel specific and channel independent cuts. In most of those cases, we use several alternative values for the cut on a particular variable. For example, we try several $\not{E}_T$ cuts, several sets of p_T cuts, etc. We employ a parameter space dependent cut optimization: at each point in SUSY parameter space, we consider all possible combinations of cuts, and determine the best combination by maximizing $S/\sqrt{B}$. In contrast to superior neural network analyses, the additional CPU requirements when employing this simple optimization are negligible. We concede that it may not be possible to perform an identical analysis with real data, particularly due to trigger issues. Even so, it is useful and interesting to see which cuts work best in the different parts of parameter space, and to see how much one can gain by choosing optimal cuts.

We first list the channel-independent cuts, which in general are designed to suppress backgrounds common to all three channels.

(1) Four $\not{E}_T$ cuts: $\not{E}_T > \{15, 20, 25\}$ GeV or no cut.

(2) Six high-end invariant mass cuts for any pair of opposite

---

[1] μ is the Higgsino mass parameter and M_2 is the soft supersymmetry breaking SU(2) gaugino mass.

[2] The assignment has been corrected in STDHEP v. 4.06.

TABLE I. Channel-specific sets of p_T cuts.

Channel	p_T cuts					
3L	$p_T(l_1)$	$p_T(l_2)$	$p_T(l_3)$	2L	$p_T(l_1)$	$p_T(l_2)$
1	11	5	5	1	11	9
2	11	7	5	2	11	11
3	11	7	7	3	13	13
4	11	11	11	4	15	15
5	20	15	10	5	20	20
	2L1T	$p_T(l_1)$		$p_T(l_2)$		$p_T(\tau)$
	1	8		5		10
	2	8		5		15
	3	11		5		10
	4	11		5		15

sign, same flavor leptons. The event is discarded if: $|M_Z - m_{l^+l^-}| < \{10,15\}$ GeV; or $m_{l^+l^-} > \{50,60,70,80\}$ GeV.

(3) Four azimuthal angle cuts on opposite sign, same flavor leptons: two cuts on the difference of the azimuthal angle of the two highest p_T leptons, $|\Delta\varphi| < \{2.5, 2.97\}$, one cut $|\Delta\varphi| < 2.5$ for *any pair* leptons, and no cut.

(4) An optional jet veto (JV) on QCD jets in the event.

We list the channel-specific p_T cuts in Table I. In the 3L channel, the first four p_T cuts in the table also require a central lepton with $p_T > 11$ GeV and $|\eta| < 1.0$ or 1.5.

For all channels we impose a low-end invariant mass cut on any pair of opposite sign, same flavor leptons, $m_{l^+l^-} > 11$ GeV. This cut is designed to suppress a number of backgrounds, e.g. Drell-Yan, $b\bar{b}$, $c\bar{c}$, and the contribution from $W\gamma^*$ (see below). It is common for lepton analyses to include a cut on the $(\Delta\eta, \Delta\varphi)$ distance between any two leptons $\Delta R > 0.4$, which suppresses background from $b\bar{b}$, $c\bar{c}$, and anomalously reconstructed cosmics. We choose not to include this cut, since we do not simulate those backgrounds. (Monte Carlo simulations do not reliably estimate the backgrounds from $b\bar{b}$ and $c\bar{c}$ production.) We have checked, however, that the effect of the ΔR cut on signal and background is negligible.

In the next section we briefly discuss the main backgrounds for the three channels. This will also motivate the choice of some of the cuts above.

III. BACKGROUNDS

We simulate the following background processes (with the generated number of events in parentheses): ZZ (10^6), WZ (10^6), WW (10^6), $t\bar{t}$ (10^6), Z+jets (8×10^6) and W+jets (8×10^6).

A. Backgrounds to the trilepton channel

We start with the WZ background, which is known to be the major source of background for the 3L channel. The total
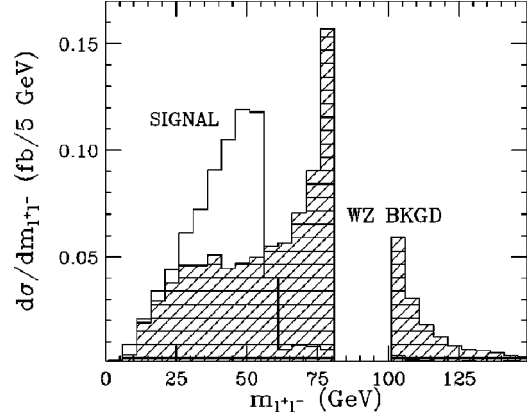

FIG. 1. The invariant mass distribution of any pair opposite sign, same flavor leptons for the signal events (with $M_0 = 700$ GeV, $M_{1/2} = 160$ GeV, $\tan\beta = 5$) and the PYTHIA WZ background. We impose a set of cuts from Ref. [14]: $p_T(l) > \{11,7,5\}$ GeV, central lepton with $p_T > 11$ GeV and $|\eta| < 1.0$, $\not{E}_T > 25$ GeV and $|m_{l^+l^-} - M_Z| > 10$ GeV. Each histogram is normalized to its cross section.

WZ cross section at run II will be ~ 2.6 pb. Folding in the branching ratios of W and Z to leptons, we get a 3L WZ background cross section production of 46 fb. It has a reducible and an irreducible component. The irreducible component (~ 3 fb) is due to $Z \to \tau^+\tau^- \to l^+l^-$ decays. The invariant mass of the resulting lepton pair from the tau decays is usually far from the Z-mass, in a region which is typical of the signal. Hence there is no obvious cut which can substantially reduce this part of the WZ background without at the same time reducing signal-to-noise. On the other hand, the remaining background (~ 43 fb) is reducible, since it arises from $Z \to l^+l^-$ decays. In this case the invariant mass $m_{l^+l^-}$ of the resulting lepton pair is equal to $p_Z^2 = (p_Z)^\mu(p_Z)_\mu$, where $(p_Z)_\mu$ is the 4-momentum of the parent boson. Most of the time the Z is produced nearly on-shell, $p_Z^2 \approx M_Z^2$. Hence, the invariant mass cut $|m_{l^+l^-} - M_Z| > 10$ GeV is very efficient in removing this source of background. However, the parent can also be off-shell, due to either the Z-width, or to $WZ/W\gamma$ interference. In PYTHIA, where only the first effect is modeled, the lepton pair invariant mass distribution follows a Breit-Wigner shape. We find that roughly 10% of the 3L background events pass the dilepton invariant mass cut, thus bringing the reducible background cross section down to about 4.3 fb. This is almost a factor of two larger than the corresponding irreducible background cross section (compare to 2.6 fb). Since ISAJET does not incorporate either Z-tail effect, we find essentially no reducible background cross section from ISAJET after the dilepton invariant mass cut is applied.[3] This difference between ISAJET and PYTHIA largely accounts for the discrepancy in the backgrounds found in Refs. [10,12] and Refs. [9,13,14]. In what follows we use PYTHIA for our background estimate.

We illustrate the above discussion in Fig. 1 where we

---

[3] Energy smearing in the detector simulation produces a very small background which survives the 10 GeV Z-mass window cut.

show the invariant mass distribution of *any* pair of opposite sign, same flavor leptons for both signal and *WZ* background. The signal point has $M_0 = 700$ GeV, $M_{1/2} = 160$ GeV and $\tan\beta = 5$, which results in $m_{\tilde\chi_1^\pm} \simeq m_{\tilde\chi_2^0} \simeq 122$ GeV. The leptons are required to pass the set of cuts from Ref. [14]: $p_T(l) > \{11,7,5\}$ GeV, central lepton with $p_T > 11$ GeV and $|\eta| < 1.0$, $\not E_T > 25$ GeV and $|m_{l^+l^-} - M_Z| > 10$ GeV. The histograms are normalized to the respective cross section.

Even with the modeling of the *Z*-width effect, we caution that the *WZ* simulation in PYTHIA is still not realistic, since the $W\gamma^*$ contribution is neglected. It results in a peak at low invariant mass, and the resulting distribution is markedly different from the result shown in Fig. 1. We anticipate that it will be necessary to cut away *all* events on the low-end of the dilepton invariant mass distribution. We therefore always apply the cut $|m_{l^+l^-}| > 11$ GeV for all three channels. This cut also helps in eliminating background lepton pairs from Drell-Yan, as well as J/ψ and Υ decays.

Since recent trilepton analyses of the Tevatron reach use ISAJET for the simulation [13,14], they underestimate the trilepton background. As a result, we find a significantly reduced Tevatron reach. However, in some cases we can employ an invariant mass cut which will substantially reduce the *WZ* background with no significant loss of signal. The signal distribution in Fig. 1 has a sharp kinematic cut-off at around $m_{\tilde\chi_2^0} - m_{\tilde\chi_1^0} \sim m_{\tilde\chi_1^\pm}/2 \sim 60$ GeV, and we can exploit this feature to increase signal-to-noise. Indeed, by applying the more stringent cut $m_{l^+l^-} < m_{\tilde\chi_1^\pm}/2 \sim 60$ GeV, we can eliminate most of the off-shell *Z* events, at almost no cost to signal. This is why in addition to standard *Z*-mass window cuts we consider four dilepton mass cuts which eliminate *all* events above a given invariant mass value. Also notice that only a very small fraction of signal events have invariant dilepton masses between 0 and 11 GeV, so that the low-end invariant mass cut $m_{l^+l^-} > 11$ GeV is quite efficient in improving $S/\sqrt{B}$. Our discussion of the *WZ* background can be similarly applied to the less serious, but nevertheless non-negligible *ZZ* background.

The second largest background to the 3L channel is from dilepton $t\bar t$ events, where there happens to be a third isolated lepton from a *b*-jet. This background is most easily suppressed by a jet veto.

Finally, the remaining 3L background one should worry about is *Z*-jet production. In this case part of the background is due to events where a jet fakes a lepton. Monte Carlo simulations, especially with a simplified detector simulation like SHW, cannot give a reliable estimate of this background. In order to estimate the fake rate one has to understand the details of the detector response as well as the jet fragmentation. Only with run II data will one be able to obtain a good estimate. For our study we follow a procedure which makes use of run I data. It was used in Ref. [20] to study the W+jets background to the 2L channel (see the next subsection).

B. Backgrounds to the like-sign dilepton channel

We now discuss the backgrounds to the 2L channel. Reference [20] observed that it can be advantageous to not re-

quire the odd-sign lepton in the 3L events due to the gain in signal acceptance. At the same time, events with two like-sign leptons are still quite rare at the Tevatron, so the 2L channel was suggested as a possible alternative to 3L for SUSY searches in run I. However, the rates for the relevant diboson backgrounds were somewhat underestimated, since ISAJET was used for the simulation. Here we are interested in determining whether the 2L channel will be useful in the larger background environment of run II.

We first do a back-of-the-envelope comparison of the *WZ* backgrounds for the 3L and 2L channels. After not requiring the odd-sign lepton, one is left with the choice of *vetoing* that lepton. In the case of a veto, we find for the relative size of the two backgrounds

$$\frac{\sigma_{WZ}(2L)}{\sigma_{WZ}(3L)} \simeq \frac{2\varepsilon_l(1-\varepsilon_l) + 0.35\varepsilon_\tau[0.65 + 0.35(1-\varepsilon_\tau)]}{2\varepsilon_l^2\varepsilon_Z + 0.35^2\varepsilon_\tau^2}$$
$$\sim \frac{1-\varepsilon_l}{\varepsilon_l\varepsilon_Z}, \tag{1}$$

where ε_l is the acceptance for leptons coming directly from *W* or *Z* decays, ε_τ is the acceptance for the (usually softer) leptons coming from leptonic tau decays, and ε_Z is the efficiency of the *Z*-window invariant mass cut: $|m_{l^+l^-} - M_Z| > 10$ GeV (we have neglected its effect on the *irreducible* background component). We find from Monte Carlo that the typical run II values for these efficiencies in *WZ* production are $\varepsilon_l \sim 0.60$, $\varepsilon_\tau \sim 0.46$ and $\varepsilon_Z \sim 0.10$. Plugging into Eq. (1), we find for the ratio 6.3, which agrees reasonably well with the result 5.8 from our full Monte Carlo simulation. For the signal point shown in Fig. 1 we find $\varepsilon_l = 0.62$ and $\varepsilon_Z = 0.99$ and the corresponding ratio is

$$\frac{\sigma_{signal}(2L)}{\sigma_{signal}(3L)} \simeq \frac{1-\varepsilon_l}{\varepsilon_l\varepsilon_Z} \sim 0.6. \tag{2}$$

This reveals that vetoing the third lepton is definitely not a good idea. In comparison to the 3L channel, the signal goes down, while the major background component is increased almost 6 times.

We therefore only consider the *inclusive* 2L channel, where we do not have any requirements on the third (odd-sign) lepton, just as in Ref. [20]. In this case, the signal acceptance is definitely increased. Unfortunately, the corresponding increase in the background is even larger than before:

$$\frac{\sigma_{WZ}(2L)}{\sigma_{WZ}(3L)} \simeq \frac{2\varepsilon_l(1-\varepsilon_l+\varepsilon_l\varepsilon_Z) + 0.35\varepsilon_\tau}{2\varepsilon_l^2\varepsilon_Z + 0.35^2\varepsilon_\tau^2} \sim 7.3 \tag{3}$$

for the typical values of the efficiencies. We can see immediately that the 2L channel can compete with the 3L on the basis of $S/\sqrt{B}$ only if the lepton acceptance for the signal is less than $1/\sqrt{7.3} \sim 37\%$. However, for typical values of the SUSY model parameters the lepton acceptance is much higher.
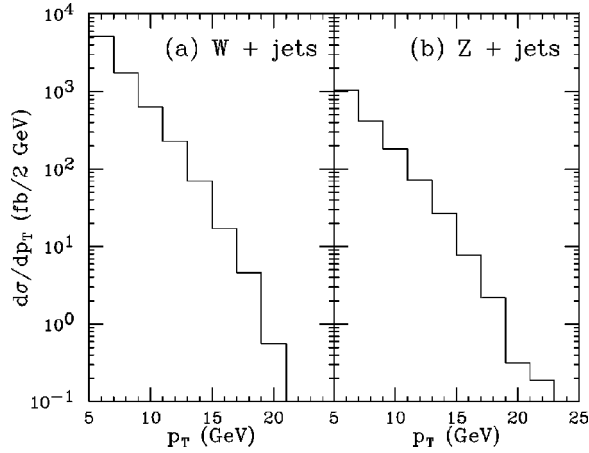
FIG. 2. p_T distribution of isolated tracks in (a) W+jet production and (b) Z+jet production. The isolated tracks have $I<2$ GeV and are outside the $\Delta R=0.7$ cone around any jet. The events in the distributions potentially contribute to the 2L background: they have one real lepton with $p_T>11$ and $|\eta|<2$ and one same sign isolated track with $|\eta|<2$.

To make matters worse, the 2L channel suffers from a potentially large new source of background: W+jet production where the jet fakes a lepton. Although the rate for a jet faking a lepton is quite small, on the order of 10^{-4}, the large W+jet cross section results in a major background for the 2L channel. As we mentioned earlier, the best way to estimate this background is from data, since Monte Carlo simulations are not reliable for fakes. In our analysis we shall follow the procedure of Ref. [20], where the rate for observing an isolated track which would otherwise pass the lepton cuts was measured in the run I Z+jet event sample. This rate was then multiplied by the probability that, given an isolated track, it would fake a lepton. This probability was measured in run I minimum bias events to be $\sim 1.5\%$, independent of p_T [20]. In our study we first simulate with Monte Carlo the p_T distribution of isolated tracks in W and Z production, which is shown in Fig. 2. In this figure we plot the isolated track p_T distribution corresponding to the 2L background, i.e. we combine a real lepton with $p_T>11$ GeV and $|\eta|<2$ with a same sign isolated track with $|\eta|<2$. Hence, the 2L

background cross section is obtained by multiplying the cross section from Fig. 2 by the probability that an isolated track will fake a lepton. We see that the background from fakes falls extremely fast with p_T, so a larger p_T requirement will substantially suppress it.

We normalize the isolated track rate to data. Using the measured 1.5% fake rate per isolated track, we find 1.5 fb of cross section when running the simulation at $\sqrt{s}=1800$ GeV and using the set of cuts from Ref. [20]. This is half the cross section found in Ref. [20]. Hence, to match the data to PYTHIA/SHW we need to double the isolated track rate obtained from Monte Carlo.

C. Backgrounds to the dilepton plus tau jet channel

The largest background to the 2L1T channel is Drell-Yan [12], where the tau jet is a fake. As it turns out, SHW does quite a good job in simulating the fake tau rate [27], so we can safely rely on the Monte Carlo for this background. We shall not further discuss the backgrounds to the 2L1T channel; we refer the interested reader to Refs. [12,28]. We find a marginal increase in the background rate here, due to the larger η coverage used in this analysis.

D. Summary and discussion

In Table II we summarize our results for the different backgrounds to the three channels.

The results are presented for a standard choice of cuts in each case. For the 3L channel, we pick the set of cuts from Ref. [14]: $p_T(l)>\{11,7,5\}$ GeV, central lepton with $p_T>11$ GeV and $|\eta|<1.0$, $\not{E}_T>25$ GeV, $|m_{l^+l^-}-M_Z|>10$ GeV, and no $|\Delta\varphi|$ or JV cuts. For the 2L channel we use the following cuts from Ref. [20]: $p_T(l)>\{11,11\}$ GeV, $|m_{l^+l^-}-M_Z|>10$ GeV, and no $\not{E}_T,|\Delta\varphi|$ or JV cuts. Here we require both leptons to have $|\eta|<2.0$, whereas Ref. [20] requires $|\eta|\lesssim1$. Finally, for the 2L1T channel we use the cuts $p_T(\tau)>15$ GeV, $|\eta(\tau)|<1.5$, $p_T(l)>\{8,5\}$ GeV, $|\eta(l)|<2.0$, $|m_{l^+l^-}-M_Z|>10$ GeV, $\not{E}_T>20$ GeV, and no JV, from Ref. [12]. All errors in the table are statistical.

Comparing to Refs. [14,20] we see a significant increase in the WZ and ZZ backgrounds in both the 3L and 2L channels. In the 2L case this is in part due to the larger η cover-

TABLE II. Background cross sections after cuts (in fb) for the three channels, each with a set of cuts described in the text. All errors are statistical. We also list the 3L background found in Ref. [14] and the 2L background found in Ref. [20].

Process	3L	[14]	2L $E=2$ TeV $\|\eta(l)\|<2$	[20] $E=1.8$ TeV $\|\eta(l)\|<1$	2L1T
ZZ	0.21 ± 0.01	0.04	1.836 ± 0.006	0.1 ± 0.01	0.372 ± 0.003
WZ	1.39 ± 0.01	0.40	8.79 ± 0.03	1.1 ± 0.02	1.36 ± 0.01
WW	0.009 ± 0.003		0.002 ± 0.001	$0+0.02$	0.54 ± 0.02
$t\bar{t}$	0.33 ± 0.01	0.14	0.21 ± 0.01	$0+0.02$	1.64 ± 0.03
Z+jet	0.13 ± 0.01		3.58 ± 0.05	1.1 ± 0.1	11.3 ± 0.6
W+jet	—		10.5 ± 0.2	3.0	
Total	2.07 ± 0.02	0.58	24.9 ± 0.2	5.6	15.2 ± 0.6

age that we use, as well as the higher center-of-mass energy. The remaining difference is due to the lack of Z-tail effects in the ISAJET simulation. The WZ background is almost as large as $W+$jet, which is not surprising based on the estimate in Eq. (3) (compare the WZ backgrounds to 3L versus 2L). We remind the reader that our 2L $W+$jet background has been normalized to the 2L $W+$jet background from Ref. [20], so the difference in the $W+$jet background seen in the table is due solely to the different tracking coverage and center of mass energy.

In the 3L case, we find significantly larger backgrounds than Ref. [14]. In fact, we surmise that the lepton efficiency is smaller in SHW than in the ISAJET detector simulation, and if one were to take this into account the background differences would be even larger. Part of the difference in the WZ and ZZ backgrounds is due to the fact that PYTHIA gives a $\sim 15\%$ larger diboson cross section than ISAJET. However, the largest part of the difference in the diboson background rates is due to the Z-width. Notice that with the fake rate procedure discussed in Sec. III B we are able to obtain an estimate of the $Z+$jet trilepton background (where the jet fakes a lepton). This background has not been taken into account in previous studies.

We do not trust the Monte Carlo simulation to provide a reliable estimate for the $W+$jet and $Z+$jet backgrounds where the jet gives rise to a real isolated lepton. We expect these backgrounds to be small, and we ignore them.

In the next section, we present results for the Tevatron reach in the three channels in the minimal gravity-mediated SUSY breaking model. In our simulations we use PYTHIA for the background estimates and ISAJET for the signal.

IV. DISCOVERY REACH FOR GRAVITY-MEDIATED MODELS

We next discuss the discovery potential of the upgraded Tevatron in the MSUGRA model. There are various SUSY production processes which give rise to the lepton signals under consideration. The dominant source of signal in most regions of parameter space is $\tilde{\chi}_1^+ \tilde{\chi}_2^0$ production. Other chargino/neutralino and slepton production processes also contribute. Typically these processes constitute a small fraction of the total signal cross section, but in some regions of parameter space (e.g. large $\tan\beta$, small M_0) they can dominate. We ignore the possibility of small contributions from squark and gluino production processes.

We first review which parts of the MSUGRA parameter space are accessible in run II via the 3L signature. The $\tilde{\chi}_1^+ \tilde{\chi}_2^0$ production cross section depends primarily on the chargino mass, and scales roughly as $M_{1/2}^{-5.5}$. Therefore, at the Tevatron we can only explore regions with small $M_{1/2}$, where the cross section is large. The $\tilde{\chi}_1^+ \tilde{\chi}_2^0$ production proceeds predominantly via s-channel W-boson exchange. There is also destructive interference from t-channel squark exchange. As a result, the $\tilde{\chi}_1^+ \tilde{\chi}_2^0$ cross section is slightly enhanced in case of heavy squarks (i.e. at large values of M_0).

At large values of M_0 ($M_0 \gtrsim 700$ GeV) the sleptons are heavy and the gauginos decay to three-body final states
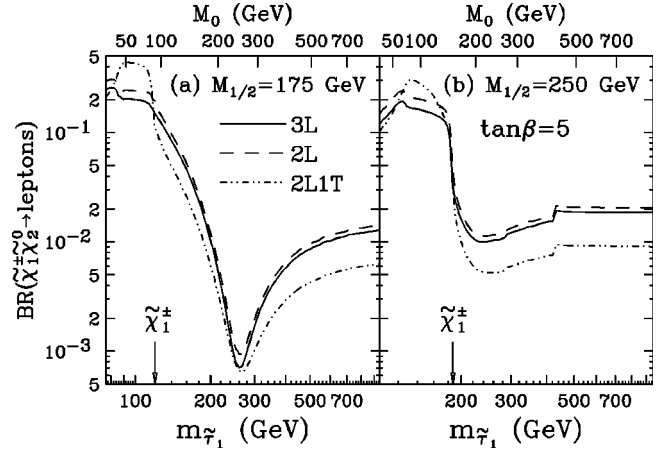

FIG. 3. Branching ratios of a chargino-neutralino pair into the 3L (solid), 2L (dash) and 2L1T (dot dot dash) channels versus the lightest stau mass (bottom axis), or alternatively, versus M_0 (top axis), with MSUGRA model parameters $\tan\beta = 5$, $\mu > 0$, $A_0 = 0$ and (a) $M_{1/2} = 175$ GeV or (b) $M_{1/2} = 250$ GeV. The arrows indicate the chargino threshold $m_{\tilde{\chi}_1^\pm} = m_{\tilde{\tau}_1}$. For the range of M_0 values shown the chargino mass varies from 118 to 139 GeV in (a), and from 187 to 201 GeV in (b).

dominantly via real (at large $M_{1/2}$) or virtual (small $M_{1/2}$) W- or Z-boson exchange. In this case the reach is determined solely by the signal production cross section. At smaller values of M_0 the off-shell slepton mediated decays destructively interfere with the gauge mediated decays. At small values of M_0 ($M_0 \lesssim M_{1/2}/2$) sleptons become lighter than the $\tilde{\chi}_1^+/\tilde{\chi}_2^0$ and two-body decays to lepton final states open up. This enhances the leptonic branching ratios of the gauginos and improves the Tevatron reach. We illustrate these features in Fig. 3 where we show the branching ratios[4] of a chargino-neutralino pair into the 3L, 2L and 2L1T channels at an MSUGRA model point with $\tan\beta = 5$, $\mu > 0$, $A_0 = 0$ and (a) $M_{1/2} = 175$ GeV or (b) $M_{1/2} = 250$ GeV. We plot versus $m_{\tilde{\tau}_1}$ (bottom axis) or M_0 (top axis). Notice that because of the rather small value of $\tan\beta$, all slepton flavors are practically degenerate.

In Fig. 3(a) the chargino mass $m_{\tilde{\chi}_1^\pm}$ is only about 120 GeV, so the two-body decay to the W-boson is closed. If $M_0 > 92$ GeV the chargino decays are three-body and the 2L and 3L channels have a larger branching ratio than the 2L1T, roughly by a factor of two. The dip in the leptonic branching ratios near $m_{\tilde{\tau}_1} \sim 260$ GeV is due to destructive interference between the Z and $\tilde{l}$-mediated graphs [30]. In the region $M_0 < 92$ GeV the two-body decays to sleptons are open and

---

[4]When we use the term "branching ratios" in relation to a pair of particles, we mean a sum of products of branching ratios. For example, if the two-body decays of $\tilde{\chi}_1^+$ and $\tilde{\chi}_2^0$ are closed, $\mathrm{BR}(\tilde{\chi}_1^+ \tilde{\chi}_2^0 \to 3L) \equiv [\mathrm{BR}(\tilde{\chi}_1^+ \to \tilde{\chi}_1^0 l^+ \nu_l) + \mathrm{BR}(\tilde{\chi}_1^+ \to \tilde{\chi}_1^0 \tau^+ \nu_\tau \to \tilde{\chi}_1^0 l^+ \nu_l \bar{\nu}_\tau \nu_\tau)][\mathrm{BR}(\tilde{\chi}_2^0 \to \tilde{\chi}_1^0 l^+ l^-) + \mathrm{BR}(\tilde{\chi}_2^0 \to \tilde{\chi}_1^0 \tau^+ \tau^- \to \tilde{\chi}_1^0 l^+ l^- \bar{\nu}_l \nu_l \bar{\nu}_\tau \nu_\tau)]$.
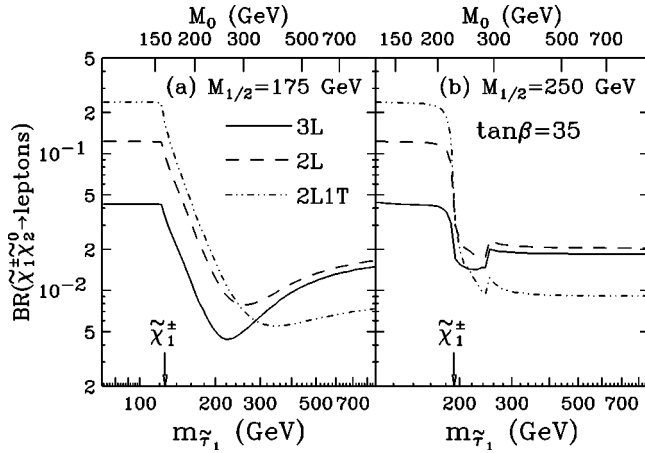
FIG. 4. The same as Fig. 3, but for $\tan\beta = 35$. This time the chargino mass varies from 126 to 140 GeV [in (a)], and from 192 to 201 GeV [in (b)].

FIG. 5. Tevatron reach in the 3L channel for MSUGRA models with $\mu > 0$, $A_0 = 0$, and (a) $\tan\beta = 5$ or (b) $\tan\beta = 35$. We show the reach with both a standard set of soft cuts [14] (dashed, for large M_0 only), as well as with the optimal set of cuts (solid) (see text). The reach is shown for 30 fb^{-1}, 10 fb^{-1} and 2 fb^{-1} total integrated luminosity (from top to bottom). The cross-hatched region is excluded by current limits on the superpartner masses. The dot-dashed lines correspond to the projected LEP-II reach for the chargino and the lightest Higgs masses. In (a) the left dotted line shows where $m_{\tilde\nu_\tau} = m_{\tilde\chi_1^\pm}$ and the right dotted line indicates $m_{\tilde\tau_1} = m_{\tilde\chi_1^\pm}$. In (b) the dotted lines show where $m_{\tilde e_R} = m_{\tilde\chi_1^\pm}$ (left) and $m_{\tilde\tau_1} = m_{\tilde\chi_1^\pm}$ (right).

quickly become dominant. But notice that while $\tilde\chi_2^0$ can decay to all slepton flavors through its B-ino component, $\tilde\chi_1^\pm$ decays dominantly to a stau, since the chargino couplings to the right-handed sleptons are proportional to the corresponding lepton masses. Hence, the branching fraction of the 2L1T channel dominates the region $40 \lesssim M_0 \lesssim 90$ GeV. For $M_0 \lesssim 40$ GeV the 2L1T branching ratio rapidly drops while the 2L and 3L branching ratios increase and become dominant again, due to two-body decays of $\tilde\chi_1^\pm$ to sneutrinos.

In Fig. 3(b) the mass of $\tilde\chi_1^\pm$ is near 190 GeV and it is always above the W-boson threshold. If M_0 is greater than about 400 GeV the $\tilde\chi_2^0$ is above the Z-boson threshold, and in this region the branching ratios for the three signatures are determined by the W- and Z-boson branching ratios to leptons. In the region $M_0 < 150$ GeV the sleptons are lighter than the chargino, and the two-body decay modes to sleptons greatly enhance the leptonic branching fractions. The 2L1T channel does not become as dominant because the chargino decays to quarks via an on-shell W-boson. The decrease in the leptonic branching ratios below $M_0 \simeq 70$ GeV is as before due to two-body decays to sneutrinos.

In Fig. 4 we show similar plots of the branching fractions, but for $\tan\beta = 35$. Many of the features seen in Fig. 3 are present here as well. For example, in Fig. 4(a) we see the broad region ($150 \lesssim m_{\tilde\tau_1} \lesssim 400$ GeV) where the destructive Z-$\tilde l$ interference severely diminishes the branching ratios. And again we observe the $\tilde\chi_2^0 \to \tilde\chi_1^0 Z$ threshold in Fig. 4(b), near $m_{\tilde\tau_1} = 260$ GeV. However, in this case the tau slepton is significantly lighter than the first two generation sleptons. Hence, the branching ratio to the three tau final state quickly approaches 100% below the stau threshold, and the 2L1T branching ratio is large. We also see that the 2L channel is competitive at small values of M_0, and is preferred over 3L on the basis of branching ratio by a factor of 2.8.

To summarize, we see that depending on the values of the MSUGRA parameters, any of the three channels offers some promise to be observed in run II. In the rest of this section, we shall do a comparative study of the three channels, ac-
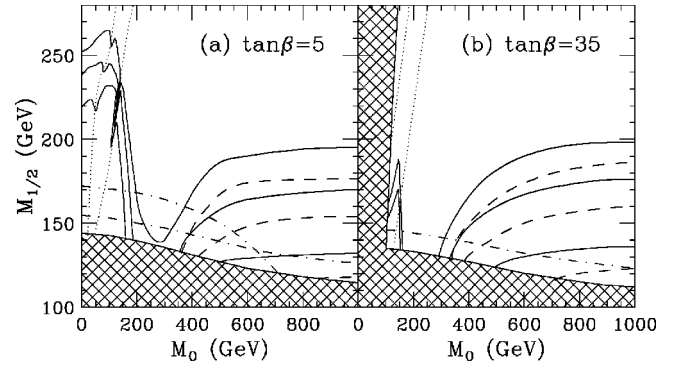
counting for all relevant background processes and using a realistic detector simulation. We shall not only update the existing 3L analyses with improved estimates of the WZ, ZZ and Drell-Yan background rates, but foremost we are interested in evaluating the different prospects each channel can offer. For example, we would like to see whether the 2L channel offers reach beyond the 3L channel, or can cover regions where the 3L channel is suppressed. Also, we want to determine the region of parameter space where the 2L1T channel can offer an independent check of a signal in one of the other channels.

The cut optimization procedure is an important ingredient in our analysis. We show results for the reach with the optimal set of cuts, determined independently at each point in SUSY parameter space. The optimal set of cuts maximizes $S/\sqrt{B}$. We require the observation of at least 5 signal events, and present our results as 3σ exclusion contours in the $M_0 - M_{1/2}$ plane, for two representative values of $\tan\beta$ – 5 and 35. We fix $\mu > 0$ and $A_0 = 0$.

In Fig. 5 we show the Tevatron reach in the 3L channel with a standard set of soft cuts [14] (dashed lines, for large M_0 only to prevent crowding), as well as with the optimal set of cuts (solid). We show the expected reach for 2, 10 and 30 fb^{-1} total integrated luminosity. The cross-hatched region is excluded by current limits on the superpartner masses and the dot-dashed lines indicate the projected reach at the CERN e^+e^- collider LEP-II for the chargino and the lightest Higgs mass.[5] In Fig. 5(a) the left (right) dotted line marks the

———

[5]It should be kept in mind that at small $\tan\beta$ the Higgs boson mass is a sensitive function of $\tan\beta$. For example, if the Higgs-boson is not discovered at LEP-II, $\tan\beta = 3, A_0 = 0$ will be excluded. The reach contours are much less sensitive to $\tan\beta$.
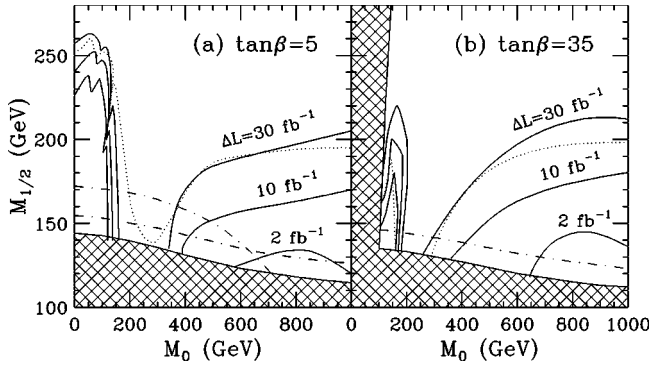
FIG. 6. The difference ΔL (in fb^{-1}) between the required total integrated luminosity for the optimal set of cuts and the default set of cuts, for the 3L signal. The three (solid) contours correspond to (from top to bottom) $\Delta L = 30$, 10 and 2 fb^{-1}. The dotted lines indicate the optimal-cut 30 fb^{-1} reach contours from Fig. 5.

$\tilde{\nu}_\tau / \tilde{\chi}_1^{\pm}$ ($\tilde{\tau}_1 / \tilde{\chi}_1^{\pm}$) mass threshold, while in Fig. 5(b) the left (right) dotted line marks the $\tilde{e}_R / \tilde{\chi}_1^{\pm}$ ($\tilde{\tau}_1 / \tilde{\chi}_1^{\pm}$) mass threshold.

Comparing to the results of Refs. [13,14], we see the Tevatron reach indicated in Fig. 5 is greatly reduced, due to the larger backgrounds found in our analysis. Even with optimized cuts our results show a much smaller observable region. For example, using the set of cuts of Ref. [14] at $\tan\beta = 35$ and $M_0 = 1$ TeV, our results indicate that the region bounded by the 2 fb^{-1} 3-σ contour extends to $M_{1/2} = 123$ GeV (or 136 GeV with optimal cuts), whereas in Ref. [14] the corresponding 5-σ region extends to 180 GeV. Similarly, their 30 fb^{-1} 3-σ contour extends to $M_{1/2} = 250$ GeV, while ours extends to $M_{1/2} = 186$ GeV (198 GeV with optimal cuts).

There is respectable reach beyond LEP-II at small values of M_0 and $\tan\beta$, where the chargino and neutralino 2-body decays to sleptons are open. As expected from Fig. 3(a), the Tevatron has no sensitivity beyond LEP-II in the region $200 \lesssim M_0 \lesssim 400$ GeV. For large values of M_0, where the leptonic decays of the gauginos are three-body, we find some sensitivity for both values of $\tan\beta$. In this region there is a clear benefit to using optimized cuts. At run II (2 fb^{-1}), with the default set of cuts, only the region with small $\tan\beta$, small M_0, and small $M_{1/2}$ can be explored beyond LEP-II. With optimal cuts, we see at large $\tan\beta$ a non-negligible region can be excluded beyond LEP-II. Looking beyond run II, we notice that at TeV33 (30 fb^{-1}) optimization can prove equivalent to doubling and sometimes even tripling the total integrated luminosity. In Fig. 6 we show the difference in the required luminosity when using the fixed set of cuts from [14] and the optimized cuts. As a guideline, we also show the 30 fb^{-1} optimal-cut contours (dotted lines) from Fig. 5.

It is instructive to examine the optimized sets of cuts. In Fig. 7 (Fig. 8) we show the optimal sets of cuts for the 3L channel in the M_0, $M_{1/2}$ plane, for $\tan\beta = 5$ ($\tan\beta = 35$). We use the following notation to describe the set of cuts at each point. The central symbol is the number of the p_T cut according to Table I. The left superscript indicates which central lepton η cut was chosen, either $|\eta| < 1.0$ (labeled "10") or $|\eta| < 1.5$ ("15"). A left subscript denotes the type
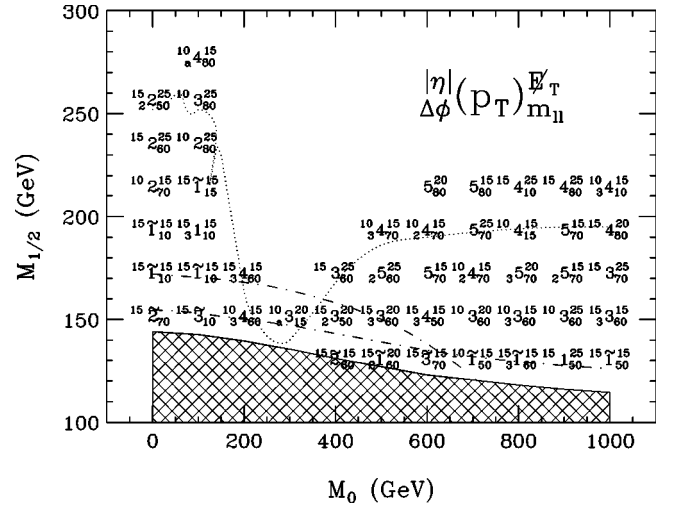

FIG. 7. The optimal sets of 3L cuts in the M_0, $M_{1/2}$ plane, for $\tan\beta = 5$. The key indicates which symbols correspond to which cuts (central lepton rapidity, $\not{E}_T$, invariant mass, $\Delta\varphi$, and p_T cuts) (see text). The dotted line indicates the optimal-cut 30 fb^{-1} reach contours from Fig. 5.

of $|\Delta\varphi|$ cut: for the two highest p_T opposite sign, same flavor leptons the $|\Delta\varphi| < 2.5$ cut is indicated by "2," the $|\Delta\varphi| < 3.0$ cut by "3," and no symbol indicates no $|\Delta\varphi|$ cut. The cut $|\Delta\varphi| < 2.5$ for *any* pair of opposite sign, same flavor leptons is indicated by "a." The right superscript shows the $\not{E}_T$ cut: $\not{E}_T > \{15,20,25\}$ GeV ("15,""20,""25"), or no cut (no symbol). A right subscript denotes the dilepton invariant mass cut: $|m_{l^+l^-} - M_Z| > \{10,15\}$ GeV ("10,""15") or $m_{l^+l^-} < \{50,60,70,80\}$ GeV ("50,""60,""70,""80"). And finally, a tilde over the central symbol indicates that the luminosity limit came from requiring 5 signal events rather than 3σ exclusion.

The jet veto cut is not indicated on the figures. However, except for one point at large $\tan\beta$ the jet veto was never selected as an optimal cut. Indeed, the major 3L background events (from WZ) are just as likely to contain extra jets as the signal.
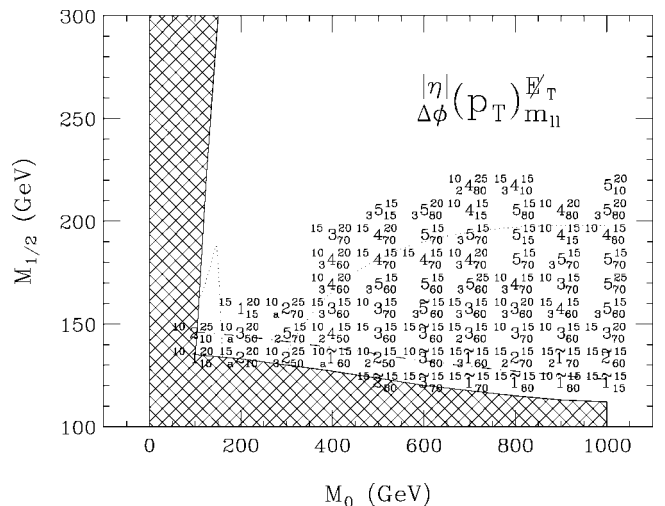

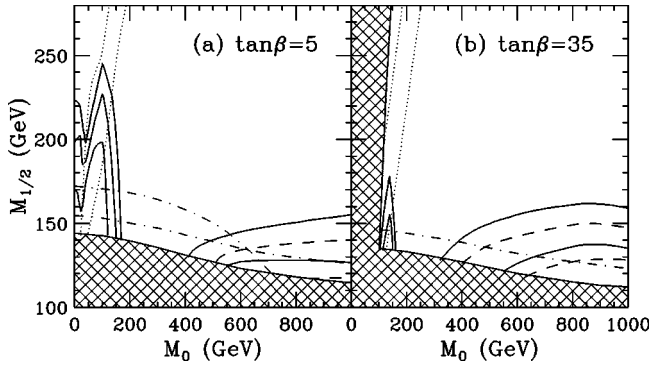FIG. 8. Same as Fig. 7, with $\tan\beta = 35$.

FIG. 9. The same as Fig. 5, for the 2L channel. The dashed lines correspond to a set of cuts from Ref. [20]. The 2, 10 and 30 fb^{-1} reach contours are plotted.
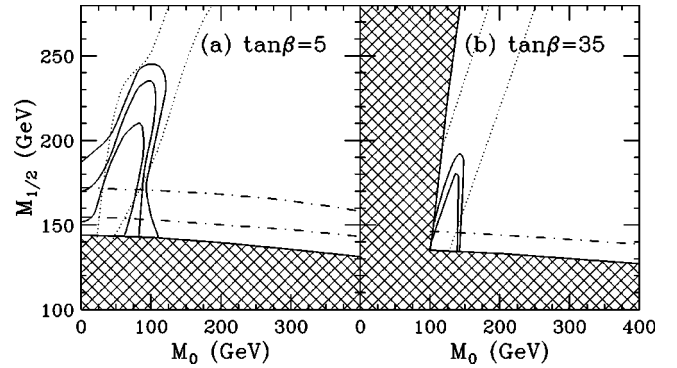

FIG. 10. The same as Fig. 5, for the 2L1T channel. In this case the optimal cuts yield very little improvement relative to a default set of cuts from Ref. [12] (listed in Sec. III D), so the contours corresponding to the default cuts are not shown.

There are several lessons to be drawn from Figs. 7 and 8. As expected, in those cases where the signal is strong and dominates over the background (typically for small $M_{1/2}$ or small M_0), softer cuts are beneficial. Indeed, the majority of the points which can be discovered with 5 signal events, have selected p_T cut "1," which is the most lenient set of p_T cuts. For larger values of $M_{1/2}$, where the background is more important, harder cuts on the lepton p_T's are preferred. In fact, we see that in the region of interest for TeV 33 at large M_0, the hardest p_T cuts we consider (from Ref. [13], indicated by "5"), often work best.

Figures 7 and 8 clearly indicate the advantage of the invariant mass cuts introduced in Sec. II. Of all the points on the plots where the background is an issue, there are only a few at which a conventional Z-mass window cut is optimal. In all other cases it is advantageous to cut all events with invariant dilepton masses above a certain threshold. Notice also how the value of the threshold tends to increase with increasing $M_{1/2}$. This is expected because the sharp edge in the signal distribution is roughly at $0.4 \cdot M_{1/2}$ (see Fig. 1).

We also see from the figures that a missing E_T cut is preferred essentially everywhere in parameter space. However, a soft $\not{E}_T$ cut ($\not{E}_T > 15$ GeV) often gives the better reach. The latest trilepton analyses [13,14] have chosen to *increase* the $\not{E}_T$ cut from its nominal run I value of 20 GeV to 25 GeV. Our results suggest that in the off-line analysis one is better off with a lower $\not{E}_T$ cut. However, more work is needed to conclusively determine what the best $\not{E}_T$ cut will be in the actual analysis. For example, triggering and energy mismeasurement issues will have to be carefully taken into account.

Lastly, in the majority of parameter space it is better not to require a $\Delta\varphi$ cut.

Looking back at Fig. 5(a), we observe that near the slepton-chargino mass thresholds the reach becomes diluted. This effect can easily be overlooked, since it only shows up very close to threshold. We find that it is entirely due to the suppressed signal acceptance. Indeed, although the branching ratio is increased immediately below threshold, the lepton resulting from the $\tilde{\chi}_2^0 \rightarrow \tilde{l}^\pm l^\mp$ decay tends to be very soft and it can fail the analysis cuts.

We next discuss the prospects for the 2L channel. In Fig.

9 we show the 2L channel reach for the Tevatron. Because of the much larger background the reach in the 2L channel is not as great as in the 3L channel. There is one important exception, however—the 2L channel does not lose sensitivity near the chargino-charged slepton threshold. Indeed, because of the Majorana nature of the neutralinos, in 50% of the events the lost soft lepton in the $\tilde{\chi}_2^0 \rightarrow \tilde{l}^\pm l^\mp$ decay is of the *opposite* sign as the charged lepton from the chargino decay. The remaining two hard leptons are then of the same sign and they are readily reconstructed. Therefore, near the $\tilde{l}/\tilde{\chi}_1^\pm$ mass threshold, the 2L channel may prove to be a valuable alternative to 3L.

Figure 5(b) reveals that at large $\tan\beta$ one starts to lose 3L sensitivity in the small M_0 region, since the decays to tau final states dominate. In fact, for $M_0 \lesssim 300$ GeV and $\tan\beta = 35$, we find no 3L reach in run II beyond LEP-II. Only with multiple years of running and collecting soft lepton events will the Tevatron be able to start improving on the LEP MSUGRA bounds. One can improve this situation by considering alternative signatures with tau jets [12]. Of those, the 2L1T channel is singled out on the basis of both sensitivity and statistical importance.

In Fig. 10 we show the Tevatron reach in the 2L1T channel. In this case we compare the optimal reach to a set of cuts from Ref. [12] (listed in Sec. III D). We find very little difference between this fixed set of cuts and the optimal set, so we do not show the fixed cut lines in the figure.

The 2L1T channel has no reach in the large M_0 region. However, when the two-body decays to staus open up the 2L1T branching fraction is larger than the other two channels, leading to some sensitivity. While the region accessible in the 2L1T channel at small $\tan\beta$ is not competitive with the 3L and 2L reach, it can improve the statistical significance in case of exclusion, or it can serve as an important confirmation and provide unique information about the model parameters in case of discovery. This channel offers the greatest reach at large $\tan\beta$ (together with the related much cleaner signature of two like-sign leptons plus a tau jet [12]) in the small M_0 region.

V. CONCLUSIONS

In this paper we studied three of the cleanest and most promising channels for SUSY discovery at the Tevatron in

run II. We revisited the trilepton and like-sign dilepton analyses, improving them in several key aspects. For example, we used a more realistic simulation of the major backgrounds. We found larger backgrounds than previous analyses. We used a procedure relying on run I data to estimate backgrounds involving fake leptons. And we introduced an invariant mass cut which took advantage of a sharp edge in the signal dilepton invariant mass distribution. This cut was generally more effective in increasing signal-to-noise than the standard invariant mass cuts. Also, we varied the cuts at each point in the supersymmetric parameter space, and determined at each point the set of cuts which yields the largest reach. We found that this cut optimization can significantly enhance the Tevatron reach. Lastly, we analyzed the reach of the 2L1T channel.

If nature is supersymmetric at low energies, and the superpartners (in particular the gauginos) are light, there is a good chance that the Tevatron will discover them in its upcoming runs. However, the 3L signature has limited reach, and we can improve the reach by optimizing cuts and considering alternative clean signatures.

Note added. We thank H. Baer for providing us with a preliminary version of a paper by H. Baer, M. Drees, F. Paige, P. Quintana and X. Tata. This paper is an update of their previous study [13] of the reach of the Tevatron in the 3L channel. Part of the improvement is the inclusion of the Z-width in the WZ background determination.

[1] P. Ramond, Phys. Rev. D **3**, 2415 (1971); Yu. A. Golf'fand and E. P. Likhtman, Zh. Eksp. Teor. Fiz., Pis'ma Red. **13**, 452 (1971) [JETP Lett. **13**, 323 (1971)]; D. V. Volkov and V. P. Akulov, Phys. Lett. **46B**, 109 (1973); J. Wess and B. Zumino, Nucl. Phys. **B70**, 39 (1974).

[2] M. Veltman, Acta Phys. Pol. B **12**, 437 (1981); E. Witten, Nucl. Phys. **B188**, 513 (1981).

[3] J. Ellis, S. Kelley, and D. Nanopoulos, Phys. Lett. B **249**, 441 (1990); U. Amaldi, W. de Boer, and H. Fürstenau, *ibid.* **260**, 447 (1991); P. Langacker and M. Luo, Phys. Rev. D **44**, 817 (1991); P. Langacker and N. Polonsky, *ibid.* **47**, 4028 (1993); P. Chankowski, Z. Płuciennik, and S. Pokorski, Nucl. Phys. **B439**, 23 (1995); J. Bagger, K. Matchev, and D. Pierce, Phys. Lett. B **348**, 443 (1995).

[4] W. de Boer, A. Dabelstein, W. Hollik, W. Mösle, and U. Schwickerath, Z. Phys. C **75**, 627 (1997); W. de Boer, R. Ehret, J. Lautenbacher, A. Gladyshev, and D. Kazakov, Report No. IEKP-KA-97-15, hep-ph/9712376; P. Chankowski, talk given at the International Workshop on Quantum Effects in the MSSM, Barcelona, 1997, hep-ph/9711470; J. Erler and D. M. Pierce, Nucl. Phys. **B526**, 53 (1998); D. M. Pierce, talk presented at the DPF Conference, Los Angeles, CA, 1999, http://www.physics.ucla.edu/dpf99/trans/1-24.pdf.

[5] K. Inoue, A. Kakuto, H. Komatsu, and S. Takeshita, Prog. Theor. Phys. **67**, 1889 (1982); R. Flores and M. Sher, Ann. Phys. (N.Y.) **148**, 95 (1983); H. Haber and R. Hempfling, Phys. Rev. Lett. **66**, 1815 (1991); Y. Okada, M. Yamaguchi, and T. Yanagida, Prog. Theor. Phys. **85**, 1 (1991); G. L. Kane, C. Kolda, and J. Wells, Phys. Rev. Lett. **70**, 2686 (1993).

[6] P. Chankowski and S. Pokorski, in *Perspectives on Supersymmetry*, edited by O. Kane (World Scientific, Singapore, 1998), hep-ph/9702431; K. Matchev and D. Pierce, Phys. Lett. B **445**, 331 (1999).

[7] LEP Electroweak Working Group, http://www.cern.ch/LEPEWWG.

[8] For a collection of recent reviews, see *Perspectives on Supersymmetry* [6].

[9] H. Baer, K. Hagiwara, and X. Tata, Phys. Rev. D **35**, 1598 (1987); T. Kamon, J. Lopez, P. McIntyre, and J. White, *ibid.* **50**, 5676 (1994); H. Baer, C.-H. Chen, C. Kao, and X. Tata, *ibid.* **52**, 1565 (1995).

[10] S. Mrenna, G. Kane, G. Kribs, and J. Wells, Phys. Rev. D **53**, 1168 (1996).

[11] D0 Collaboration, S. Abachi *et al.*, Phys. Rev. Lett. **76**, 2228 (1996); CDF Collaboration, F. Abe *et al.*, *ibid.* **76**, 4307 (1996); B. Abbott *et al.*, *ibid.* **80**, 1591 (1998); F. Abe *et al.*, *ibid.* **80**, 5275 (1998).

[12] J. Lykken and K. Matchev, Report No. FERMILAB-PUB-99/034-T hep-ph/9903238.

[13] H. Baer, C.-H. Chen, M. Drees, F. Paige, and X. Tata, Phys. Rev. Lett. **79**, 986 (1997); Phys. Rev. D **58**, 075008 (1998).

[14] V. Barger, C. Kao, and T.-J. Li, Phys. Lett. B **433**, 328 (1998); V. Barger and C. Kao, FERMILAB-PUB-98/342-T hep-ph/9811489.

[15] TeV 2000 Report, FERMILAB-PUB-96/082.

[16] V. Barger, T. Han, D. Zeppenfeld, and J. Ohnemus, Phys. Rev. D **41**, 2782 (1990); S. Frixione, P. Nason, and G. Ridolfi, Nucl. Phys. **B383**, 2 (1992); J. Ohnemus, Phys. Rev. D **44**, 3477 (1991); **47**, 940 (1993); **50**, 1931 (1994).

[17] R. Meng, G. A. Schuler, J. Smith, and W. L. van Neerven, Nucl. Phys. **B339**, 325 (1990); P. Nason, S. Dawson, and R. K. Ellis, *ibid.* **B303**, 607 (1988); **B327**, 49 (1989); W. Beenakker, H. Kuijf, W. L. van Neerven, and J. Smith, Phys. Rev. D **40**, 54 (1989).

[18] G. Altarelli, R. K. Ellis, and G. Martinelli, Nucl. Phys. **B157**, 461 (1979); S. Mrenna, UCD-99-4 hep-ph/9902471.

[19] M. Krämer, talk given at the Higgs and Supersymmetry Conference, Gainesville, FL, 1999, http://www.phys.ufl.edu/ rfield/higgs_susy.html.

[20] J. Nachtman, D. Saltzberg, and M. Worcester, hep-ex/9902010.

[21] T. Sjöstrand, Comput. Phys. Commun. **82**, 74 (1994); S. Mrenna, *ibid.* **101**, 232 (1997).

[22] F. Paige, S. Protopopescu, H. Baer, and X. Tata, Report No.

BNL-HET-98-39, hep-ph/9810440.

[23] J. Conway, talk given at the SUSY/Higgs Workshop meeting, Fermilab, 1998. See also www.physics.rutgers.edu/jconway/soft/shw/shw.html.

[24] S. Jadach, J. H. Kuhn, and Z. Was, Comput. Phys. Commun. **64**, 275 (1990); **76**, 361 (1993).

[25] CDF Technical Design Report, FERMILAB-PUB-96/390-E.

[26] L. Garren, STDHEP manual, http://www-pat.fnal.gov/stdhep.html.

[27] K. Matchev, talk given at the Higgs and Supersymmetry Con-ference, Gainesville, FL, 1999.

[28] Report of the SUGRA Working Group, to appear in the Pro-ceedings of the SUSY/Higgs Workshop, Fermilab.

[29] A. Chamseddine, R. Arnowitt, and P. Nath, Phys. Rev. Lett. **49**, 970 (1982); H. Nilles, Phys. Lett. **115B**, 193 (1982); L. Ibáñez, *ibid.* **118B**, 73 (1982); R. Barbieri, S. Ferrara, and C. Savoy, *ibid.* **119B**, 343 (1982).

[30] H. Baer and X. Tata, Phys. Rev. D **47**, 2739 (1993); H. Baer, C. Kao, and X. Tata, *ibid.* **48**, 5175 (1993).